Mechanical Systems and Signal Processing 126 (2019) 521–535

Contents lists available at ScienceDirect

Mechanical Systems and Signal Processing

journal homepage: www.elsevier.com/locate/ymssp

Real-time combustion torque estimation and dynamic misfire fault diagnosis in gasoline engine

Taixiong Zheng [a,*], Yu Zhang [a], Yongfu Li [a], Lichen Shi [b]

[a] Center for Automotive Electronics and Embedded System, Chongqing University of Posts and Telecommunications, Chongqing 400065, PR China
[b] Unit 63963 of PLA, Beijing 100072, China

ARTICLE INFO

Article history:
Received 7 September 2017
Received in revised form 17 February 2019
Accepted 24 February 2019
Available online 2 March 2019

Keywords:
Gasoline engine
Misfire fault diagnosis
Engine combustion torque
Luenberger sliding mode observer

ABSTRACT

In this research, an innovative state observer of gasoline engine based on the combination of Luenberger and sliding mode technique is proposed. This state observer is designed to track crankshaft angular speed and estimate engine combustion torque based on the experimental crankshaft angular speed of a four-cylinder Spark Ignition (SI) engine. Then, a new advance in the application of Artificial Neural Networks (ANNs) based on the estimated results of automated dynamic misfire fault diagnosis both under steady state and non-stationary condition is discussed in detailed. In order to effectively obtain data for network training, the estimated engine combustion torque is segmentally preprocessed according to the crank angle displacement of automobile engine. Furthermore, a series of experiments are carried out under normal and a variety of misfire conditions. The ANN systems are trained and tested using prepared cases. Finally, the Back-Propagation Neural Network (BPNN), Elman Neural Network (ENN), and Support Vector Machine (SVM) are applied to diagnose misfire fault, the effectiveness of each is evaluated respectively. Based on the estimated engine combustion torque, the experimental results show that the designed ENN is able to correctly diagnose misfire fault with a running time of 0.6 s, including single misfire, intermittent double-cylinder misfire, and continuous double-cylinder misfire in transient working condition.
© 2019 The Authors. Published by Elsevier Ltd. This is an open access article under the CC BY-NC-ND license (http://creativecommons.org/licenses/by-nc-nd/4.0/).

1. Introduction

Engine misfire is a phenomenon that the cylinder does not ignite normally due to mechanical or electronic failure. Misfire Fault Diagnosis (MFD) of automotive engine is an important issue in On Board Diagnosis (OBD) system, which has significant impacts on vehicle movement, such as emissions, fuel consumption, and engine damage. The effective detection of misfire events can promote energy conservation and reduce economic loss caused by incomplete combustion and the damage of three-way catalytic converter [1], etc. According to the basic requirements of common work cycle of gasoline engine in practical operation, misfire can be caused by a variety of factors, namely bad fuel quality, electromagnetic interference, system fault of exhaust gas recirculation, poor ignition, insufficient fuel supply, mechanical failure, etc. Therefore, it is substantially challenging to detect misfire events among the above-mentioned causes. The process of MFD includes three phases: (i) make a judgment whether there is a misfire fault or not; (ii) if misfire event exists, identify its causes; (iii) estimate the severity of

* Corresponding author.
E-mail address: zhengtx@cqupt.edu.cn (T. Zheng).

https://doi.org/10.1016/j.ymssp.2019.02.048
0888-3270/© 2019 The Authors. Published by Elsevier Ltd.
This is an open access article under the CC BY-NC-ND license (http://creativecommons.org/licenses/by-nc-nd/4.0/).

Nomenclature

T_{eng}	Engine torque
λ	Air to fuel ratio
θ	Crank angle
ω	Crankshaft angular speed
$\ddot{\theta}$	Crank angular acceleration
A_ξ	Spark advance (degrees before top-dead-center)
m_ϑ	The mass of air entering into intake manifold for combustion in cylinder
P_{in}	Engine intake manifold pressure
J_e	Engine crankshaft effective rotational moment of inertia
T_{load}	Engine load torque
T_{aero}	Aerodynamic resistance torque
T_β	Road grade and rolling resistance torque
T_{fb}	Friction brake torque
C_q	Aerodynamic drag coefficient
r_g	Engine crankshaft total gear ratio
g_t	The transmission gear ratio
g_{fd}	The final drive gear ratio
r_w	The wheel radius
β	Road grade
μ	Coefficient of rolling resistance
g	The acceleration due to gravity
M	The mass of vehicle;
v	Vehicle speed
F_{fb}	The brake force on the vehicle is applied to the conventional friction brake
T_{com}	Engine combustion torque
R	Crankshaft radius
l	The length of connecting rod
T_r	Reciprocating inertia torque
T_{frc}	The average friction torque
$\Omega_1, \Omega_2, \Omega_3, \Omega_4$	The segmental section of each engine cylinder
$\hat{T}_{com}^{1n_1}, \hat{T}_{com}^{1n_2}, \hat{T}_{com}^{1n_3}, \hat{T}_{com}^{1n_4}$	Engine combustion torque of each segmental section
n_1, n_2, n_3, n_4	The number of engine combustion torque of each segmental section
$X_{\max}$	Maximum of original data
$X_{\min}$	Minimum of original data
$Z_{\max}$	The upper bound of normalization
$Z_{\min}$	The lower bound of normalization;
l_1	The number of neuron in input layer
l_2	The number of neuron in hidden layer
k	The serial number of ENN calculation process
N	The total number in the test group

misfire. Hence, a complete process of misfire diagnosis is composed of these three steps. This study is focused on detecting misfire events and their locations in misfire cylinder(s).

Numerous techniques of misfire detection have been proposed in existing literatures [2–4]. Different methods of MFD based on the effect of missing combustion on engine behavior have been investigated since 1980. In 2001, Merkisz [4] comprehensively summarized the methods of MFD and analyzed the difficulties in implementation. In 2003, the application of Fault Detection and Isolation (FDI) procedure was systematically described by Venkatasubramanian [5–7], which includes quantitative model-based methods, qualitative models, and history-based methods. In 2008, Ding [8] summarized the strategy and development of fault diagnosis technology from the perspective of model-based methods. Additionally, with the transition of production technology from 2010 to 2012, automobile manufacturer was required to detect complete single misfire events, results in the introduction of MFD of new energy vehicles. Further, in 2013, the range of MFD was extended to multi-cylinder misfire fault and intermittent misfire under all working conditions. However, MFD remains to be challenging especially when multi-cylinder misfire events occur under high speed and low load condition, in which case, due to the effect of increasing process variables on diagnosis accuracy, the number of misfire cylinder is difficult to detect in transient operating condition.

In general, the engine MFD methods can be categorized into in-cylinder combustion diagnosis and post-cylinder combustion diagnosis [9]. There are three ways to detect in-cylinder combustion: direct measurements of ion current signal, optical signal, and in-cylinder pressure signal. The first method is designed to monitor relatively few procedure parameters, such as chamber pressure and air-fuel ratio, by using the probe integrated with a spark plug. The value of ion current indicates that the absence of combustion in the cylinder possibility due to misfire events. The study in reference [10] analyzed the characteristics of ion current signal under misfire condition and achieved reliable MFD. The method which uses optical sensor for MFD is mainly applied in experimental study [4]. The primary method is to process the in-cylinder pressure data measured by conventional piezoelectric sensors [11]. The estimated cylinder pressure and deviation torque based on Sliding Mode Observer (SMO) have been used to develop the diagnosis system of misfire fault [12,13].Unfortunately, the estimator was not designed in transient condition. Furthermore, based on the strong correlation of in-cylinder pressure signal, reference [14] offered a promising misfire detection solution using ANN when the misfire event occurred in Homogeneous Charge Compression Ignition (HCCI) engine with ethanol as a renewable fuel. However, the proposed method is difficult to achieve due to poor chamber environment and high cost of sensor. Additionally, these aforementioned signals are not practical in use for on-board MFD.

The second category of MFD is based on the measurements of post-cylinder parameters, including crankshaft angular speed, crankshaft angular acceleration, crankshaft angle displacement, engine combustion torque, engine block vibration signal, exhaust gas properties, engine noise signal, oxygen sensor signal, Engine Roughness (ER), etc. The signals, such as crank shaft angular speed, crankshaft angular acceleration, and crankshaft angle displacement, are commonly used in production engines [15]. Lee [16] developed a misfire detection system using ANN with a revised synthetic angular acceleration as input. Although, this system was validated to be reliable, it is noted that these signals contained a large amount of noises caused by the sensor errors, the change of dynamic load, and the road condition. Engine block vibration signal and engine noise signal generally blend together to post challenges in finding the appropriate technique to distinguish them [17]. Compare to the traditional Fast Fourier Transform (FFT), the proposed Wavelet Analysis (WA) technique in reference [18] is more effective in filtering out high-frequency components of engine block vibration signals in misfire and normal combustion. Study [19] illustrated the use of Decision Tree (DT) as a tool for feature extraction on the basis of indirect information in vibration signal of the engine block. The acquired feature was further applied to detect misfire cylinder. Additionally, a novel nonlinear analysis method using Lyapunov exponents based vibroacoustic exhaust signals was put forward to develop the on-board MFD system in locomotive engine [20]. This method has a good real-time performance in steady condition. Analysis of exhaust gas pressure and composition, temperature measurements before and inside a catalytic converter has been used for misfire detection [21–23], but these methods were based on exhaust gas properties with typically low response time. In order to avoid the tendency of falling into local optimal solution and relatively low diagnostic accuracy, Yuan and Tian [24,25] presented an excellent strategy using the Improved Particle Swarm Optimization (IPSO) algorithm to optimize Support Vector Machine (SVM), which can be further applied to diagnose misfire fault. Reference [26] put forward a new technique to detect the misfire of diesel engine based on exhaust noise using statistical simulation method (Bootstrap), which yields the confidence interval and histogram of required feature values. But the key issue of this method is to effectively choose the failure characteristics reflecting the difference under types of conditions. Oxygen sensor signal measured by wide-band oxygen sensors installed at the confluence point of the exhaust ports has been used to measure the variation in oxygen concentration [27]. This method could possibly be a good choice for misfire detection. ER was recently proposed to present the variation of crankshaft angular acceleration evaluate the operation condition of engine and detect misfire events [28] . Paper [29] proposed an interacting multiple model for misfire detection based on estimated combustion torque using Parametric Kalman Filtering (PKF). This model is capable effectively detecting the actual cylinder state early in the early combustion phase. However, the aforementioned MFD methods have not been conducted in transient condition yet.

Since the post-cylinder parameters, such as crankshaft angular speed and crankshaft angular acceleration, are greatly affected by sensor errors, the change of dynamic load, and road condition, the factors related to the in-cylinder ignition events are considered. Given that engine combustion torque is directly related to in-cylinder ignition events, it is beneficial to base the misfire detection and misfire cylinder allocation judgment on [30]. Therefore, it is used as the focus of this study. However, engine combustion torque cannot be directly measured by sensors. Therefore in this study, the method of indirect estimation is taken into consideration in this study [31]. Given that SMO has good robustness and accuracy in parameters estimation, SMO is chosen as the tool to elaborate engine combustion torque. Additionally, the estimated results need to be further disposed by MFD. Considering the advantages of simple structure and mature technique, ANN has been widely applied in classification and function approximation fields. ANN has very strong nonlinear mapping, self-organizing, and self-adaption capability, which makes ANN a good choice for MFD [32].

This study is motivated by the great challenge in multiple cylinders MFD in transient working condition. In this study, an Optimized Luenberger Sliding Mode Observer (OLSMO) is proposed and used to estimate dynamic engine combustion torque in transient condition. For the design of the state observer of engine combustion torque, a rigid crankshaft model is used underlie the role of crankshaft angular speed tracking error. The designed OLSMO is validated both experimentally (on the four-cylinder engine) and theoretically (the convergence of observer). Then, the estimated engine combustion torque is used for MFD under steady state and non-stationary condition. Furthermore, an ANN based system is developed to automatically diagnose misfire events in four-cylinder SI engine. In particular, the obtained engine combustion torque is segmentally processed in correspondence with the crank angle displacement of automobile engine, then applied to train and test network. In order to validate the designed networks for MFD, three methods including BPNN, ENN, and SVM are used to

make a comparison. Meanwhile, a series of experiments are carried out both under normal condition and with a variety of misfire events. Finally, the results show that the automatic diagnostic system, especially ENN, based on estimated engine combustion torque, can detect misfire events efficiently, including single misfire, intermittent double-cylinder misfire, and continuous double-cylinder misfire, even under transient working condition. ENN is capable of correctly diagnose misfire fault with a relative higher accuracy compared to SVM, and its convergence curve is smoother than BPNN, which indicates that ENN has a strong robustness in misfire detection for gasoline engine.

The rest of the paper is organized as follows. The rigid crankshaft model is described in Section 2; an optimized Luenberger sliding mode observer is designed and the estimated results are presented in Section 3; the method of MFD using ENN is proposed and the results of MFD are discussed in Section 4; finally, conclusions are reached in Section 5.

2. Rigid crankshaft model

In this section, the dynamic system of rigid engine crankshaft model is briefly described. According to the engine model of SI engine proposed by Crossley and Cook [33], the engine torque produced by the engine cylinders can be expressed in the form of polynomial function

$$T_{eng} = \varphi(\lambda) + \psi(\omega, A_\zeta) + H(m_\vartheta, A_\zeta) \tag{1}$$

where the functions $\varphi(\lambda)$, $\psi(\omega, A_\zeta)$, and $H(m_\vartheta, A_\zeta)$ are defined respectively, as follows

$$\begin{cases} \varphi(\lambda) = a\lambda^2 + b\lambda + \varepsilon \\ \psi(\omega, A_\zeta) = c\omega^2 + d\omega + \eta\omega A_\zeta \\ H(m_\vartheta, A_\zeta) = \tau A_s^2 + fA_\zeta + hA_\zeta^2 m_\vartheta + iA_\zeta m_\vartheta + jm_\vartheta \end{cases} \tag{2}$$

where $a, b, \varepsilon, c, d, \lambda, \tau, f, h, i, j$ are polynomial coefficients which need to be calibrated via bench test according to specified engine type. Furthermore, m_ϑ can also be expressed in the form of polynomial function

$$m_\vartheta = F(\omega, P_{in}) = \alpha\omega + \sigma\omega P_{in}^2 + o\omega^2 P_{in} + pP_{in}^2 + qP_{in} \tag{3}$$

where α, σ, o, p, q are polynomial coefficients needed to be determined.

Additionally, the engine torque subtracts the net load torque equals to acceleration.

$$J_e\ddot{\theta} = T_{eng} - T_{load} \tag{4}$$

where engine load torque T_{load} can be approximately described as three main factors including (i) aerodynamic resistance torque T_{aero}, (ii) road grade and rolling resistance torque T_β, and (iii) friction brake torque T_{fb} [34]. The engine speed is proportional to the vehicle speed, e.g., $v = \omega r_g$ as long as the wheels do not slip. Thus, T_{aero} is given by $T_{aero} = C_q r_g^3 \omega^2$, where $r_g = r_w / g_t g_{fd}$. The torque as a function of road grade β and rolling resistance coefficient μ, can by expressed as $T_\beta = (-\mu Mg\cos\beta + Mg\sin\beta) r_g$. And $T_{fb} = F_{fb} r_g$ is the retarding torque caused by force F_{fb} applied to the vehicle's conventional friction brake [35–36]. Therefore, the load torque can be denoted as

$$T_{load} = T_{aero} - T_\beta + T_{fb} \tag{5}$$

According to the crankshaft dynamic system of the multi-cylinder gasoline engine, the dynamic equation of the crankshaft rotation can be described as

$$J_e\ddot{\theta} = T_{com} - T_r - T_{frc} - T_{load} \tag{6}$$

where engine combustion torque T_{com}, reciprocating inertia torque T_r, and average friction torque T_{frc} are analyzed in detail in reference [37]. Further, the Eq. (6) can also be represented as

$$T_{com} = J_e\ddot{\theta} + T_r + T_{frc} + T_{load} \tag{7}$$

Define the state variables $x_1 = \theta, x_2 = \omega$, then Eq. (4) can be transformed into the state space

$$\begin{cases} \dot{x}_1 = x_2 \\ \dot{x}_2 = \frac{1}{J_e}(T_{eng} - T_{load}) \end{cases} \tag{8}$$

Substitute Eq. (1) into the state space, Eq. (8) can be derived as

$$\begin{cases} \dot{x}_1 = x_2 \\ \dot{x}_2 = \frac{1}{J_e}[\varphi(\lambda) + \psi(x_2, A_\zeta) + H(m_\vartheta, A_\zeta) - T_{load}] \end{cases} \tag{9}$$

3. Observer design and estimated results

3.1. Optimized Luenberger sliding mode observer design

In this study, the sliding surface, which is the switching function, is chosen as

$$s = x_2 - \hat{x}_2 \tag{10}$$

where $\hat{x}_2$ is the estimation of the measured speed x_2. Based on the principle of sliding mode variable structure, formula (10) is applicable condition when $s\dot{s} < 0$. In order to meet the sliding mode condition, the effective injection signal needs to be chosen. During the sliding mode motion, the well-chosen switching function could be equal to zero due to discontinuous injection signals. Therefore, the system yields excellent robustness under disturbance signals and uncertain condition. Additionally, the better sharp saturation function is applied to weaken the vibration in switching function attacking crank angular speed. Then, the derivative of switching function is obtained

$$J_e\dot{s} = J_e\left(\dot{x}_2 - \dot{\hat{x}}_2\right) = E(s) - \mathrm{K}sat(s/\varepsilon),\ (\mathrm{K} > 0) \tag{11}$$

where $E(s)$ represents the error function between the designed observer and stiff crankshaft model, $\mathrm{K}sat(s/\varepsilon)$ is a designed injection signal, Kis the sliding mode gain, $sat(\cdot)$ is a saturation function, and ε is a positive constant. The slope of the linear part in $sat(s/\varepsilon)$ is $1/\varepsilon$ which should be large enough to approach to sign function. Meanwhile, in order to ensure that the switching function convergence fast, the sliding mode gain should be as big as possible. However, if K has an excessively large value, the vibration in switching function will increase and decrease the accuracy in tracking speed. Therefore, a Luenberger observer is further introduced to accelerate the estimating speed of estimated states. And Eq. (11) can be improved as

$$J_e\dot{s} = E(s) - [Ls + \mathrm{K}sat(s/\varepsilon)],\ (\mathrm{K}, L > 0) \tag{12}$$

where L is Luenberger gain. According to the estimated speed $\hat{x}_2$, the optimized Luenberger sliding mode observer of crankshaft dynamics in Eq. (9) can be rewritten as

$$\begin{cases} \dot{\hat{x}}_1 = \hat{x}_2 \\ \dot{\hat{x}}_2 = \frac{1}{J_e}[\varphi(\lambda) + \psi(\hat{x}_2, A_\zeta) + H(\hat{m}_\vartheta, A_\zeta) - T_{load}] + Ls + \mathrm{K}sat(s/\varepsilon) \end{cases} \tag{13}$$

where $\hat{m}_\vartheta = F(\hat{x}_2, P_{in}) = \alpha\hat{x}_2 + \sigma\hat{x}_2P_{in}^2 + o\omega^2P_{in} + pP_{in}^2 + qP_{in}$. And the estimated crank angular acceleration can be obtained

$$\hat{y} = \dot{\hat{x}}_2 \tag{14}$$

Substitute Eq. (13) into the Eq. (7), the estimated combustion torque can be obtained

$$\hat{T}_{com} = \varphi(\lambda) + \psi(\hat{x}_2, A_\zeta) + H(\hat{m}_\vartheta, A_\zeta) + \hat{T}_r + \hat{T}_{frc} + Ls + \mathrm{K}sat(s/\varepsilon) \tag{15}$$

where

$$\hat{T}_r = m_{pc}\left[\hat{y}L_e(x_1) + R^2\hat{x}_2^2G(x_1)\right]L_e(x_1) \tag{16}$$

$$\hat{T}_{frc} = \frac{\left(y_c\hat{x}_2^2 + u\hat{x}_2 + z\right)V_d}{\pi k_{cyl}} \tag{17}$$

3.2. Stability analysis

According to Eqs. (9) and (13), the designed Luenberger sliding mode observer is utilized to continuously track crank angular speed by changing the estimated combustion torque. Now define error function of Luenberger observer as

$$J_e\dot{s} = \psi(x_2, A_\zeta) - \psi(\hat{x}_2, A_\zeta) + H(m_\vartheta, A_\zeta) - H(\hat{m}_\vartheta, A_\zeta) - Ls \tag{18}$$

Additionally, substitute $\psi(x_2, A_\zeta), \psi(\hat{x}_2, A_\zeta), H(m_\vartheta, A_\zeta), H(\hat{m}_\vartheta, A_\zeta), m_\vartheta$ and $\hat{m}_\vartheta$ with, the above formula can be expressed as

$$J_e\dot{s} = \left[d + \eta A_\zeta + (j + iA_\zeta + hA_\zeta^2)[(o(x_2 + \hat{x}_2)P_m + \sigma P_m^2 + \alpha] - c(x_2 + \hat{x}_2) - L\right]s \tag{19}$$

Define

$$A = d + rA_f + (j + iA_f + hA_f^2)[(o(x_2 + \hat{x}_2)P_m + nP_m^2 + m] + c(x_2 + \hat{x}_2) - LC \tag{20}$$

where $C = 1$. Then Eq. (19) can be rewritten as

$$\dot{s} = \frac{1}{J_e}(A - LC)s \tag{21}$$

By means of Lyapunov stability theorem, if the characteristic matrix of Luenberger observer satisfies the Hurwitz condition, which specifies that a negative real part exists in the eigen value of $(A-LC)$, the asymptotic stability of the error dynamics is guaranteed. Therefore, we can derive

$$\det[\lambda I-(A-LC)]=|\lambda-(A-LC)|=\lambda-A+L=0 \tag{22}$$

where I represents the unit matrix. Since λ is less than zero, $A-L<0$. Therefore, we can derive Luenberger gain $L>A$. Additionally, refer to Eqs. (12) and (20), error dynamic system can be expressed as

$$\dot{s}=\frac{(A-L)s-\mathrm{K}sat(s/\varepsilon)}{J_e} \tag{23}$$

A Lyapunov function candidate is selected as $V=(1/2)s^2$. By differentiating both sides of Lyapunov function, the derivative of the Lyapunov function is obtained as $\dot{V}=s\dot{s}$. Apparently, the inequality $\dot{V}<0$ holds true based on Lyapunov theorem.

$$\dot{V}=s\dot{s}=s\frac{(A-L)s-\mathrm{K}sat(s/\varepsilon)}{J_e}<0 \tag{24}$$

The above formula proves that Eq. (23) is stable if a proper gain $\mathrm{K}>(A-L)s$ is selected.

3.3. Experimental results of engine combustion torque estimation

In this experiment setup, a four-cylinder SI engine (details are listed in Table 1) is used in real-time torque estimation study. And the value of the aforementioned polynomial coefficients of four-cylinder SI engine are calibrated in bench test according to the specified engine model in Table 1, the polynomial coefficients of which are shown in Table 2.

In order to achieve the proposed observer using optimized Luenberger sliding mode technique, a dynamic engine platform is conducted under unsteady condition. The crankshaft angular speed and crank angle are experimentally measured using angular velocity sensor. The operational state of the vehicle is set to New European Drive Cycle (NEDC), which has been widely applied to exam the transient emission. Additionally, the crank speed signal is extracted by crankshaft position sensor, and sampling frequency of signal is chosen to be 20 kHz. The flowchart of the experimental process using OLSMO with observer gain $K=60, L=120$ is shown in Fig. 1. In this figure, the designed observer has six inputs, including crank speed, crank angle, fraction torque, reciprocating inertia torque, load torque, and tracking speed error. Finally, the estimated engine combustion torque is an output which is used to MFD. If the estimated engine combustion torque decreases dramatically in a full engine cycle, it is considered a misfire fault is detected and the details are discussed in Section 4 for ANN Design Scheme.

In this section, the estimated results of idle mode, acceleration mode, and deceleration mode using OLSMO are presented respectively in the next few figures. And the estimated results are based on partial experiment data of NEDC condition within a minute. The tracking results of crankshaft angular speed are given in Fig. 2, which shows a good overall performance of OLSMO in speed tracking without strong vibration during steady state in Graph (a), acceleration state in Graph (b) and deceleration state in Graph (c) under NEDC condition. Additionally, the speed tracking error of OLSMO from cool start process to 25 s ending is given in Graph (d). The steady state error (from 7 to 10 s) is close to zero, and the speed tracking error is only 3% in transient state (for example: from 11 to 15 s). Therefore, Graph (d) indicates that the proposed observer possesses have achieved good stability.

Table 1
Features and specifications of turbocharged SI engine.

Parameter	Value and Unit
Engine Type	4-cylinder 4-stroke in-line
Firing Order	1-3-4-2
Engine Capacity	2.0 L
Compression Ratio	10.5:1
Bore	83 mm
Crank Radius	93/2 mm
Connecting Rod Length	145 mm

Table 2
The polynomial coefficients of four-cylinder SI engine.

Coefficient	Value	Coefficient	Value	Coefficient	Value	Coefficient	Value
a	−0.85	b	21.91	c	−0.000107	d	0.027
τ	0.0028	f	0.26	η	0.00048	h	−0.05
i	2.55	j	379.36	ε	−181.3	α	−0.0000783
σ	−0.0337	o	0.0001	p	−0.0725	q	0.1812
y_c	5×10^{-8}	u	0.00015	z	0.97		

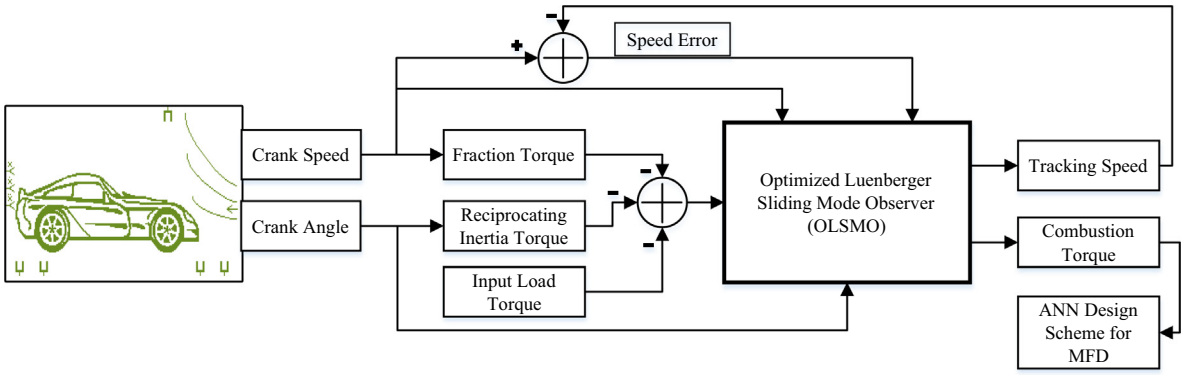

Fig. 1. Flowchart of experimental process.

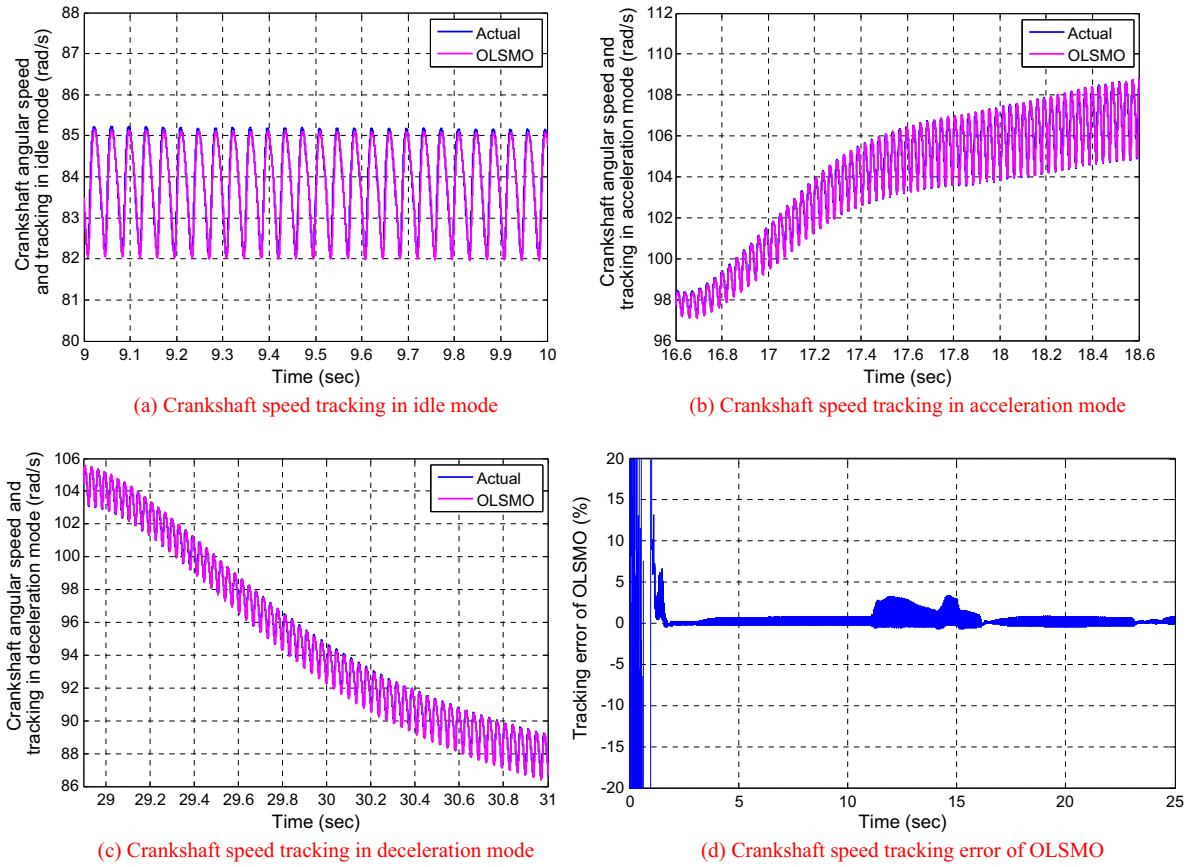

(a) Crankshaft speed tracking in idle mode

(b) Crankshaft speed tracking in acceleration mode

(c) Crankshaft speed tracking in deceleration mode

(d) Crankshaft speed tracking error of OLSMO

Fig. 2. Crankshaft angular speed tracking results using OLSMO in NEDC.

Fig. 3 shows the experimental results of estimator under different working condition including (a) Free fault condition in idle mode, (b) Misfire in cylinder 2 in acceleration mode, (c) Misfire in cylinder 4&1 in acceleration mode, and (d) Misfire in cylinder 1&3 in deceleration mode. A great reduction of combustion torque in cylinder 2 can be seen in subplot (b) and the irregular sharp reduction of combustion torque in cylinder 4&1 is shown in subplot (c). Further, the estimated engine combustion torque matches that of the measured one under different working conditions, which indicates that the designed OLSMO is well capable of constructing the actual engine combustion torque under both steady condition and transient working condition. It is assumed that OLSMO has good robustness and can effectively decrease the influence of external disturbance and system uncertainty. Therefore, it is concluded that the proposed OLSMO holds a good dynamic performance in estimating engine combustion torque. Further, the numbers in Fig. 3 represent the engine cylinder sequence under different

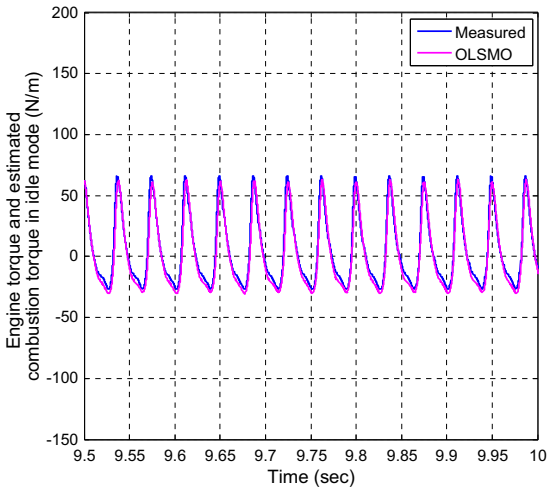

(a) Engine torque estimated with free fault condition in idle mode

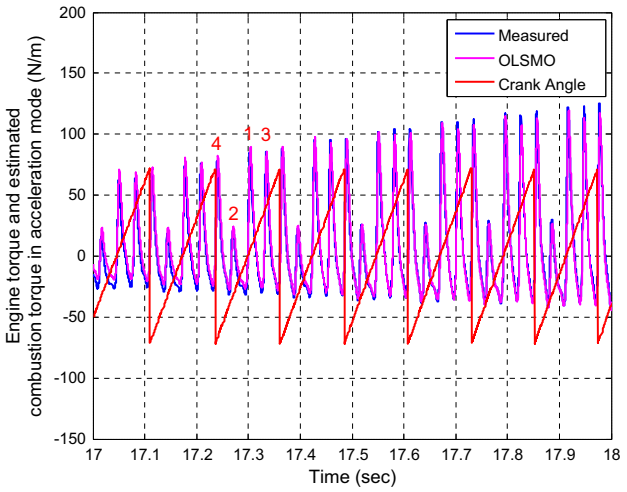

(b) Engine torque estimated with misfire in cylinder 2 in acceleration mode

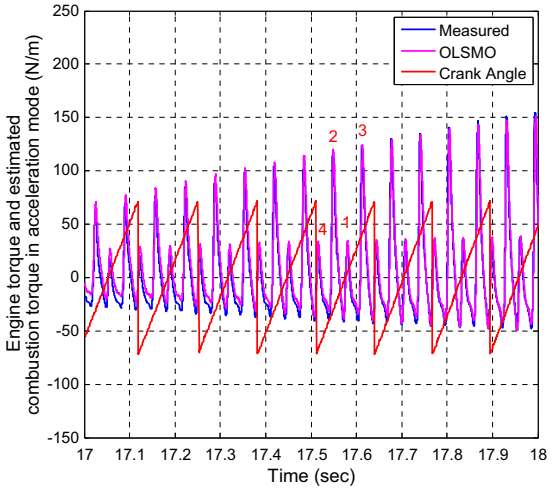

(c) Engine torque estimated with misfire in cylinder 4&1 in acceleration mode

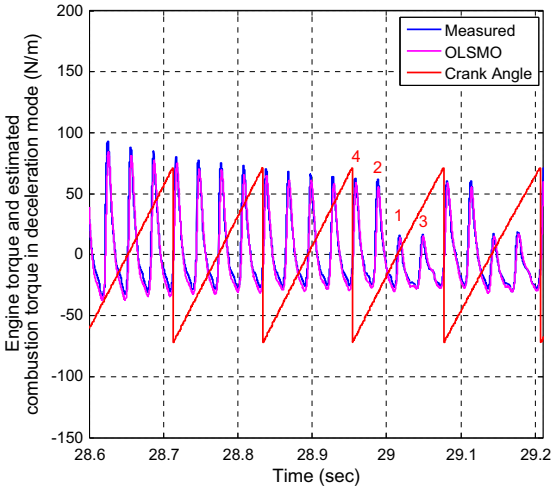

(d) Engine torque estimated with misfire in cylinder 1&3 in deceleration mode

Fig. 3. Estimated results of engine combustion torque using OLSMO.

working condition. It can be seen that the characteristics of misfire is obvious for each cycle when misfire event occurs. It is verified that the estimated engine combustion torque can be applied to MFD.

4. ANN for misfire fault diagnosis

4.1. Feature extraction

Numerous studies have shown that ANNs can effectively differentiate various faults of rotating machines [33,34]. Based on a considerable amount of training data, the designed ANN can make a decent judgment on given inputs which have never been presented before. In order to efficiently train the designed networks, the estimated results need to be further disposed. According to the experimental crankshaft angle displacement of engine, the estimated engine combustion torque is divided into four segments at the valley value of amplitude in each cycle with 720 degrees. As shown in Fig. 4, the approximate summation of engine combustion torque for each cylinder is acquired in this section.

The curve of crank angle is the crankshaft angle displacement of engine, which is processed by modular arithmetic with 720 degrees. In this case, the rotation position of engine crankshaft can be determined based on the location of Top Dead Center (TDC) in cylinder 1, which indicates that the engine crankshaft sequentially rotates certain angle when the rotation

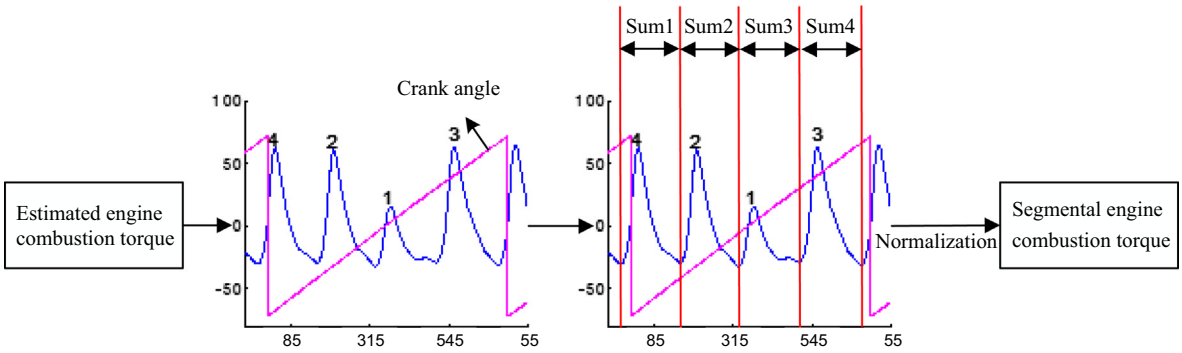

Fig. 4. Treatment scheme of estimated engine combustion torque.

position is allocated via TDC of cylinder 1. The expression is described in formula (25), where *mod* $(\cdot)$ represents the function of modular arithmetic and *angular* is the crank shaft angle displacement. The expression is multiplied by 0.2 to decrease the weight of angle displacement.

$$Crank\_angle = 0.2 * [\ mod\ (angular, 720) - 360] \tag{25}$$

Given the input $\hat{T}_{com}$ in treatment scheme, the segmental data based on combustion cycle of each engine cylinder are defined as

$$\begin{cases} \Omega_1 : \hat{T}^{11}_{com}, \hat{T}^{12}_{com}, \cdots, \hat{T}^{1n_1}_{com} \\ \Omega_2 : \hat{T}^{21}_{com}, \hat{T}^{22}_{com}, \cdots, \hat{T}^{2n_2}_{com} \\ \Omega_3 : \hat{T}^{31}_{com}, \hat{T}^{32}_{com}, \cdots, \hat{T}^{3n_3}_{com} \\ \Omega_4 : \hat{T}^{41}_{com}, \hat{T}^{42}_{com}, \cdots, \hat{T}^{4n_4}_{com} \end{cases} \tag{26}$$

According to study [1], the summation of engine combustion torque in each segmental section are defined as

$$\begin{cases} \hat{T}^{1}_{com} = \sum_{\kappa=1}^{n_1} \hat{T}^{1\kappa}_{com} \\ \hat{T}^{2}_{com} = \sum_{\kappa=1}^{n_2} \hat{T}^{2\kappa}_{com} \\ \hat{T}^{3}_{com} = \sum_{\kappa=1}^{n_3} \hat{T}^{3\kappa}_{com} \\ \hat{T}^{4}_{com} = \sum_{\kappa=1}^{n4} \hat{T}^{4\kappa}_{com} \end{cases} \tag{27}$$

In order to eliminate the differences in data attributed to the neural network training process, the segmental engine combustion torque is further normalized. Define segmental engine combustion torque as $X = \left[\hat{T}^{1}_{com} \quad \hat{T}^{2}_{com} \quad \hat{T}^{3}_{com} \quad \hat{T}^{4}_{com}\right]$, the rule of normalization is given as

$$Y = \frac{(Z_{max} - Z_{min}) \times (X - X_{min})}{X_{max} - X_{min}} + Z_{min} \tag{28}$$

where Z_{max} and Z_{min} can be adjusted. The normalization interval is set to $[-1,\ 1]$ in this section. Therefore, Z_{max} and Z_{min} is defined as -1 and 1, respectively.

4.2. Structure design of ENN

Though BPNN is successfully applied in fault diagnosis field with its strong nonlinear mapping capability, its convergence speed is still slow and may not converge to a global minimum compared to the feedback networks, such as ENN. Therefore, the ENN is experimentally used to detect misfire in this section.

The ENN consists of four layers: input layer, hidden layer, context layer, and output layer. The engine loads are taken into consideration and the system inputs are from normalized data by feature extraction using summation of estimated combustion torque for each combustion cylinder in one cycle. Thus, the input layer of ENN has 4 neurons. The number of neurons in hidden layer of ENN is determined by a trial and error procedure. In general, the relation to the number of neurons between hidden layer and input layer approximation can be denoted as:

$$l_2 = 2l_1 + 1 \tag{29}$$

Table 3
9 operation conditions of engine.

Working Condition	Fault Code	Classification label
Normal condition	[0 0 0 1]	1
Misfire in cylinder 1	[0 0 1 0]	2
Misfire in cylinder 2	[0 0 1 1]	3
Misfire in cylinder 3	[0 1 0 0]	4
Misfire in cylinder 4	[0 1 0 1]	5
Misfire in cylinder 1&3	[0 1 1 0]	6
Misfire in cylinder 4&2	[0 1 1 1]	7
Misfire in cylinder 1&4	[1 0 0 0]	8
Misfire in cylinder 3&2	[1 0 0 1]	9

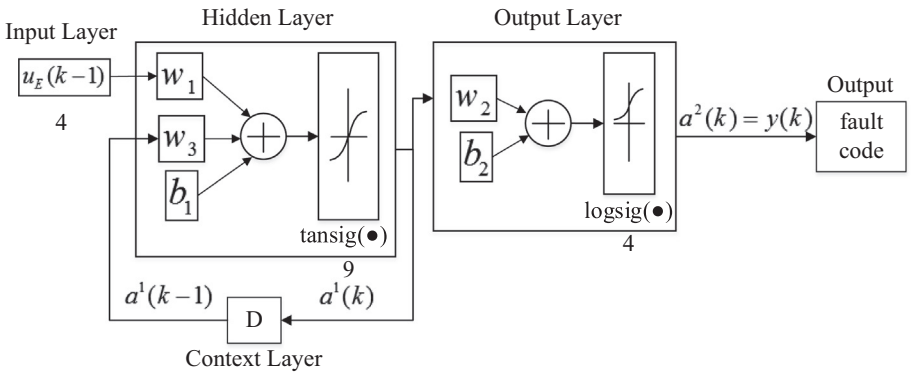

Fig. 5. The diagram of the ENN with hyperbolic tangent and logistic regression transfer functions.

Therefore, the number of neurons in hidden layer is set to 9. The context layer describes a feedback process which contains a feedback value from hidden layer. The output layer has 4 neurons and the output value of each neuron is either 0 or 1, which represents 9 misfire conditions from [0 0 0 1] to [1 0 0 1], respectively as shown in Table 3.

In particular, since the ignition order is set to 1-3-4-2, misfire in cylinder 1&3 and 4&2 represent double cylinder continuous misfire fault condition. And misfire in cylinder 1&4 and 3&2 represent double cylinder intermittent misfire fault condition.

As shown in Fig. 5, the diagram of the ENN is designed to obtain the desired target. Both input and output vector have 4-dimension. The output vector of hidden layer and context layer have 9-dimension. w_1, w_2, w_3 are connection weights of the input layer to hidden layer, hidden layer to output layer, and context layer to hidden layer, respectively. b_1 and b_2 are threshold value of hidden layer and output layer. And tan$sig(\cdot)$ is hyperbolic tangent transfer function, log $sig(\cdot)$ is logistic regression transfer function.

Define the input vector of ENN as

$$u_E(k-1) = \left[\bar{\hat{T}}^1_{com} \quad \bar{\hat{T}}^2_{com} \quad \bar{\hat{T}}^3_{com} \quad \bar{\hat{T}}^4_{com} \right] \tag{30}$$

Then the output vector of hidden layer can be expressed as

$$a^1(k) = \tan sig(w_1 u_E(k) + w_3 a^1(k-1) + b_1) \tag{31}$$

Based on the output of hidden layer, the context layer is added to a delayer, therefore, $a^1(k-1)$ represents the output of context layer. The output of output layer can be expressed as

$$a^2(k) = y(k) = \log sig(w_2 a^1(k) + b_2) \tag{32}$$

where $y(k)$ is the practical output of ENN.

4.3. Learning process of ENN

The procedure parameters are defined in the learning process of ENN. The ENN is trained up to 1000 epochs (net. epochs = 1000) to achieve the discrepancy of 0.001 (net.goal = 0.001). The training status is displayed for every 10 epochs (net.show = 10). The learning rate is set to 0.1 (net.lr = 0.1) and the momentum constant is set to 0.9 (net.mc = 0.9).

Define the error function as

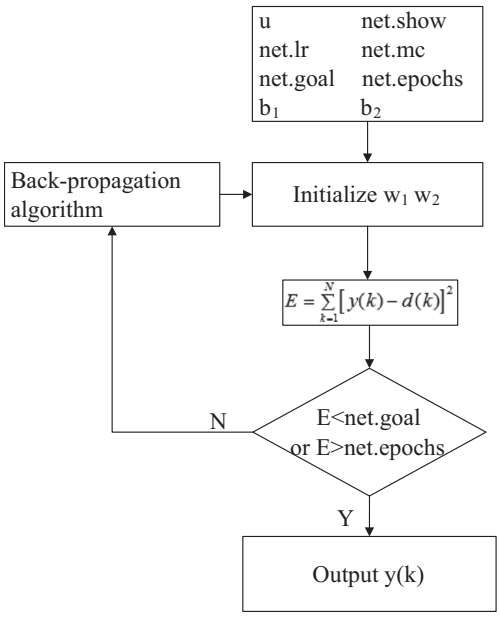

Fig. 6. The flowchart of the ENN training process with back-propagation algorithm.

$$E(k) = \frac{1}{2}\sum_{k=1}^{N}[y(k) - d(k)]^2 \tag{33}$$

where $d(k)$ is the desired output. Additionally, the connection weights and threshold value of hidden layer and output layer are revised via the back-propagation algorithm. Thus, the training process of ENN is presented in Fig. 6.

4.4. Evaluation index

In order to evaluate the performance of designed ENN, two fitness criterions *error_ratio* and *res* are introduced as follow

$$error\_ratio = \frac{\sum_{k=1}^{N}|y(k) - d(k)|}{N} \tag{34}$$

$$res = norm\left(\sum_{k=1}^{N}|y(k) - d(k)|\right) \tag{35}$$

where $norm(\cdot)$ represents the matrix norm, *error_ratio* represents the average error ratio in output value and target value, and *res* is the norm of error which indicates that *res* is a distance metric in Euclidean space. A higher fitness criterion means poorer ENN performance.

4.5. Experimental results

In this study, ENN is used to detect different misfire events and the methods of SVM and BPNN are also introduced to validate the performance of designed ENN. Additionally, three engine working conditions, which includes idle mode (approximately 800 rpm), acceleration mode (920 rpm–1150 rpm), and deceleration mode (1015 rpm–820 rpm), are designed for the automatic MFD. There are a total of 108 cases for each working condition and all cases are from the experiments on four-cylinder SI engine (details are listed in Table 1). Furthermore, each working condition is divided into two

Table 4
The distribution of data under different misfire condition.

For Training/For Test	Idle/Acceleration/Deceleration Mode			
Normal	6 in total			
Single Misfire	6 in cylinder 1	6 in cylinder 2	6 in cylinder 3	6 in cylinder 4
Double Cylinder Misfire	6 in cylinder 1&3	6 in cylinder 4&2	6 in cylinder 1&4	6 in cylinder 3&2

Table 5
The output results of ENN.

Output label	Practical output results	Desire output results	Engine real state	Classification results
$y(1)$	[0.0474 0.0451 0.0866 0.9787]	[0 0 0 1]	Normal	True
$y(7)$	[0.0344 0.0003 0.9941 0.0001]	[0 0 1 0]	Misfire in cylinder 1	True
$y(13)$	[0.0300 0.0172 0.9800 0.9981]	[0 0 1 1]	Misfire in cylinder 2	True
$y(19)$	[0.0118 0.9972 0.0267 0.0057]	[0 1 0 0]	Misfire in cylinder 3	True
$y(25)$	[0.0290 0.9936 0.0098 0.9737]	[0 1 0 1]	Misfire in cylinder 4	True
$y(31)$	[0.0000 0.9497 0.9628 0.0014]	[0 1 1 0]	Misfire in cylinder 1&3	True
$y(37)$	[0.0064 0.9628 0.9772 0.9996]	[0 1 1 1]	Misfire in cylinder 2&4	True
$y(43)$	[0.9266 0.0050 0.0181 0.0052]	[1 0 0 0]	Misfire in cylinder 1&4	True
$y(49)$	[0.9693 0.0024 0.0193 0.9983]	[1 0 0 1]	Misfire in cylinder 2&3	True

groups, one for networks training (54 cases), the remaining 54 cases are for test purposes. The distribution of different misfire conditions is shown in Table 4.

The results of MFD under acceleration condition using ENN are presented in Table 5. Since the test process contains 54 data sets, the partial results of ENN are shown in Table 5. In particular, the practical output of ENN is turned into a binary code according to the rounding rules. The results show that the ENN can accurately diagnose different misfire fault.

Furthermore, the value of the ENN fitness criterion is calculated under acceleration condition. According to formula (34) and (35), the fitness criterion can be expressed as $error\_ratio = 0.0921$ and $res = 0.3843$. The results show that the value of fitness criterion is very small. Therefore, the designed ENN is capable of accurately diagnosing the misfire fault in multi-cylinder.

Since the BPNN and SVM are introduced to make a comparison in MFD, the experimental results of BPNN and SVM are also presented in this study. As shown in Table 6, the partial test results of BPNN indicate that the test case of output label $y(9)$ is incorrectly diagnosed. In this case, the practical output is [1 0 1 0], which shows that the result of MFD is abnormal.

Table 6
The output results of BPNN.

Output label	Practical output results	Desire output results	Engine real state	Classification results
$y(1)$	[0.0318 0.0280 0.0422 0.9913]	[0 0 0 1]	Normal	True
$y(9)$	[0.5953 0.0194 0.8923 0.0083]	[0 0 1 0]	Misfire in cylinder 1	False
$y(13)$	[0.0171 0.0246 0.9983 1.0000]	[0 0 1 1]	Misfire in cylinder 2	True
$y(19)$	[0.0109 0.9949 0.0450 0.0039]	[0 1 0 0]	Misfire in cylinder 3	True
$y(25)$	[0.1177 0.9947 0.0000 0.8774]	[0 1 0 1]	Misfire in cylinder 4	True
$y(31)$	[0.0042 0.9776 0.9930 0.0003]	[0 1 1 0]	Misfire in cylinder 1&3	True
$y(37)$	[0.0001 0.9633 0.9781 1.0000]	[0 1 1 1]	Misfire in cylinder 2&4	True
$y(43)$	[0.9976 0.0260 0.0039 0.0836]	[1 0 0 0]	Misfire in cylinder 1&4	True
$y(49)$	[0.9957 0.0026 0.0267 0.9957]	[1 0 0 1]	Misfire in cylinder 2&3	True

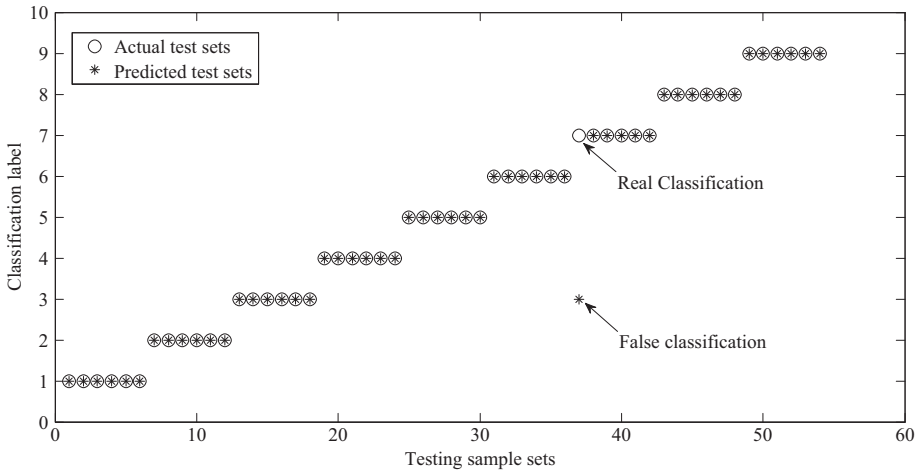

Fig. 7. Test results of misfire fault diagnosis using SVM (Deceleration condition).

Table 7
A performance comparison of MFD.

Working Condition	Performance	BPNN	ENN	SVM	MLP [38]
Idle Mode	Error Ratio	0.1041	0.1318	–	0.4941
	Res	1.2054	1.4049	–	–
	Running Time	0.6510 s	0.6172 s	0.2601 s	–
	Accuracy	52/54	52/54	52/54	36/36
Acceleration Mode	Error Ratio	0.1380	0.0921	–	–
	Res	0.9410	0.3843	–	–
	Running Time	0.6214 s	0.5600 s	0.3022 s	–
	Accuracy	53/54	54/54	53/54	–
Deceleration Mode	Error Ratio	0.0473	0.0873	–	–
	Res	0.2388	0.6665	–	–
	Running Time	0.6042 s	0.4938 s	0.2730 s	–
	Accuracy	54/54	54/54	53/54	–

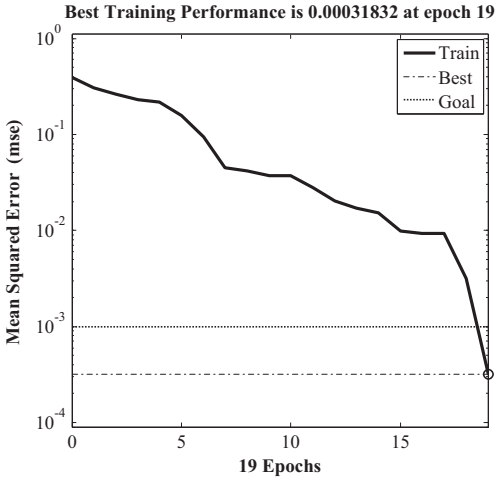

Fig. 8. Training process of BPNN.

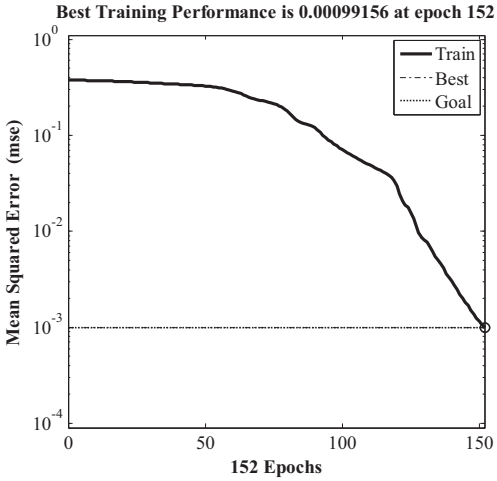

Fig. 9. Training process of ENN.

The value of BPNN fitness criterion is calculated under acceleration condition. The fitness criterion $error\_ratio = 0.1380$ and $res = 0.9410$. Compared to the designed ENN, the value of BPNN fitness criterion is larger, which leads to a larger discrepancy in MFD than the designed ENN. However, BPNN is relatively accurate in multi-cylinder misfire fault diagnosis.

The experimental results of SVM under deceleration condition are presented in Fig. 7, which displays 54 test data sets in MFD and only one error occurs during test process. In this case, the test result of the seventh classification (Misfire in cylinder 2&4) is incorrectly diagnosed as the fourth classification (Misfire in cylinder 3).

The final results for performance comparison of MFD under different working condition are shown in Table 7.

Firstly, the results of MFD are analyzed from the perspective of detection accuracy. Compare BPNN and SVM to the designed ENN, the designed ENN is more accurate in misfire diagnosis performance and the results show that the test case is incorrectly classified only under idle condition. However, the introduced SVM and BPNN are unable to realize MFD perfectly and one error occurred in MFD under different engine operation condition. In particular, the method of engine misfire fault diagnosis proposed by Jian Chen [38] is based on Multi-Layer Perceptron networks (MLPs) using torsional vibration signal of crankshaft. Though the accuracy of MFD using MIP is higher than ENN under idle condition, the MLP is only applied in single misfire fault diagnosis.

Secondly, the results of MFD are analyzed from the perspective of running time. The results show that the SVM consumes the least amount of time in MFD, which is only 0.3*s*. However, ENN and BPNN take about 0.6*s* in MFD, and the running time of ENN is shorter than that of BPNN. Though SVM takes the shortest running time in MFD, its misfire fault diagnosis accuracy is lower than ENN and BPNN under transient condition. Therefore, ENN has an advantage over engine misfire fault diagnosis compared to BPNN and SVM.

Finally, with regard to the fitness criterion, the designed ANNs including BPNN and ENN have a better performance in MFD under idle condition compared to MLP. Further, the value of fitness criterion using BPNN is larger than that of ENN under acceleration condition. Which shows that ENN has a better performance for multi-cylinder misfire fault diagnosis.

Additionally, though the value of fitness criterion of BPNN is smaller than ENN under idle and deceleration condition, the experimental results in Table 7 shows that ENN is also accurate in detecting misfire event without affecting practical application. Furthermore, according to the comparison between Figs. 8 and 9, for ENN, the error curve of training process is smoother than that of BPNN, which indicates that the introduced feedback in ENN has improved the stability of the network. Thus, the ENN is capable of detecting misfire fault with greater practical value and effectively avoid the local optimal solution. In conclusion, ENN has a superior overall performance in MFD.

5. Conclusion

An automatic dynamic MFD system is developed in this paper. The method of obtaining estimated engine combustion torque based on optimized Luenberger sliding mode observer and effectively designing artificial neural networks using estimated results are studied. The proposed estimator is applied to track crankshaft speed and estimate engine combustion torque based on experimental crankshaft angular speed of a four-cylinder SI engine. The inputs of the ANNs are proposed segmental data according to crankshaft angle displacement of engine. The simulated outcomes of BPNN, ENN, and SVM methods in MFD are compared. It is demonstrated that the proposed automatic diagnostics system has a better performance compared to the designed MLP in work [38]. Additionally, from the final results, though the designed SVM and BPNN are not as robust as the ENN, these three methods can efficiently detect and diagnose various misfire events under transient working condition. More importantly, the proposed ENN is superior to BPNN in the aspect of obtaining a strongly effectively performance in misfire detection for gasoline engine.

Acknowledgments

This work is jointly supported by Chongqing Natural Science Foundation (Grant No. cstc2018jcyjA0629), Chongqing Natural Science Foundation of Education Commission (Grant No. KJ120511).

References

[1] M.A. Rizvi, A.I. Bhatti, Q.R. Butt, Hybrid model of the gasoline engine for misfire detection, IEEE Trans. Ind. Electron. 58 (8) (2011) 3680–3692.
[2] J. Mohammadpour, M. Franchek, K. Grigoriadis, A survey on diagnostics methods for automotive engines, in: Proceedings of American Control Conference, IEEE, San Francisco, CA, 2011, pp. 985–990.
[3] J. Mohammadpour, M. Franchek, K. Grigoriadis, A survey on diagnostic methods for automotive engines, Int. J. Engine Res. 13 (1) (2012) 41–64.
[4] J. Merkisz, P. Bogus, R. Grzeszczyk, Overview of engine misfire detection methods used in on board diagnostics, J. KONES 8 (1) (2001) 326–341.
[5] V. Venkatasubramanian, R. Rengaswamy, K. Yin, S. Kavuri, A review of process fault detection and diagnosis: Part I: Quantitative model-based methods, Comput. Chem. Eng. 27 (3) (2003) 293–311.
[6] V. Venkatasubramanian, R. Rengaswamy, K. Yin, S. Kavuri, A review of process fault detection and diagnosis: Part II: Qualitative models and search strategies, Comput. Chem. Eng. 27 (3) (2003) 313–326.
[7] V. Venkatasubramanian, R. Rengaswamy, K. Yin, S. Kavuri, A review of process fault detection and diagnosis: Part III: Process history based methods, Comput. Chem. Eng. 27 (3) (2003) 327–346.
[8] S.X. Ding, Model-based Fault Diagnosis Techniques, Springer-Heidelberg, Berlin, 2008, pp. 1–11.
[9] M. Boudaghi, M. Shahbakhti, S.A. Jazayeri, Misfire detection of spark ignition engines using a new technique based on mean output power, J. Eng. Gas Turbines Power 137 (9) (2015).
[10] Q. Fan, J. Bian, H. Lu, S. Tong, L. Li, Misfire detection and re-ignition control by ion current signal feedback during cold start in two-stage direct-injection engines, Int. J. Engine Res. 15 (1) (2012) 37–47.
[11] J.M. Luján, V. Bermúdez, C. Guardiola, A. Abbad, A methodology for combustion detection in diesel engines through in-cylinder pressure derivative signal, Mech. Syst. Sig. Process. 24 (7) (2010) 2261–2275.

[12] J. Molinarmonterrubio, R. Castrolinares, Sliding mode observer for internal combustion engine misfire detection, in: Proceedings of Electronics, Robotics and Automotive Mechanics Conference, IEEE, Morelos, 2007, pp. 620–624.
[13] Y.S. Wang, F.L. Chu, Real-time misfire detection via sliding mode observer, Mech. Syst. Sig. Process. 19 (4) (2005) 900–912.
[14] B. Bahri, A.A. Aziz, M. Shahbakhti, M.F.M. Said, Understanding and detecting misfire in an HCCI engine fuelled with ethanol, Appl. Energy 108 (8) (2013) 24–33.
[15] M. Gevecia, W.O. Andrew, A.F. Matthew, An investigation of crankshaft oscillations for cylinder health diagnostics, Mech. Syst. Sig. Process. 19 (5) (2005) 1107–1134.
[16] M. Lee, M. Yoon, M. Sunwoo, S. Park, K. Lee, Development of a new misfire detection system using neural network, Int. J. Automot. Technol. 7 (5) (2006) 637–644.
[17] B. Li, P.L. Zhang, Z.J. Wang, S.S. Mi, P.Y. Liu, Morphological covering based generalized dimension for gear fault diagnosis, Nonlinear Dyn. 67 (4) (2012) 2561–2571.
[18] J. Chang, K. Manshik, M. Kyoungdoug, Detection of misfire and knock in spark ignition engines by wavelet transform of engine block vibration signals, Meas. Sci. Technol. 13 (7) (2002) 1108–1114.
[19] S.B. Devasenapati, V. Sugumaran, K.I. Ramachandran, Misfire identification in a four-stroke four-cylinder petrol engine using decision tree, Expert Syst. Appl. 37 (3) (2010) 2150–2160.
[20] P. Bogus, M. Jerzy, Misfire detection of locomotive diesel engine by non-linear analysis, Mech. Syst. Signal Process. 19 (4) (2005) 881–899.
[21] S. Kim, C. Minho, S. Kooksang, The misfire detection by the exhaust pressure ascent rate, Trans. Korean Soc. Automot. Eng. 11 (2) (2003) 1–7.
[22] Z.F. Li, Y. He, Study on fault diagnosis model of misfire in engines based on rough set theory and neural network technology, Trans. Chin. Soc. Agri. Mach. 36 (08) (2005) 118–121.
[23] M. Tamura, H. Saito, Y. Murata, K. Kokubu, S. Morimoto, Misfire detection on internal combustion engines using exhaust gas temperature with low sampling rate, Appl. Therm. Eng. 31 (17–18) (2011) 4125–4131.
[24] R.D. Yuan, D. Peng, H.Z. Feng, M. Hu, Fault diagnosis for engine by support vector machine and improved particle swarm optimization algorithm, J. Info. Comput. Sci. 11 (13) (2014) 4827–4835.
[25] J. Tian, H. Gu, Anomaly detection combining one-class SVMs and particle swarm optimization algorithms, Nonlinear Dyn. 61 (1) (2010) 303–310.
[26] W. Kang, X.Y. Qiao, G. An, Method of diagnosis diesel engine misfire fault based on statistical simulation, Chin. Internal Combust. Engine Eng. 25 (05) (2004) 66–68.
[27] Y.S. Wang, Diagnosing electron-controlled gasoline engine default by exhaust gas sensor, J. Traffic Transp. Eng. 02 (2002) 48–51.
[28] S. Naik, Advanced misfire detection using adaptive signal processing, Int. J. Adapt Control Signal Process. 18 (2) (2004) 181–198.
[29] S. Helm, M. Kozek, S. Jakubek, Combustion torque estimation and misfire detection for calibration of combustion engines by parametric kalman filtering, IEEE Trans. Ind. Electron. 59 (11) (2012) 4326–4337.
[30] A.K. Sood, A.A. Fahs, N.A. Henein, Engine fault analysis: Part II—Parameter estimation approach, IEEE Trans. Ind. Electron. 32 (4) (1985) 301–307.
[31] W.J. Wang, Z.T. Wu, J. Chen, Fault identification in rotating machinery using the correlation dimension and bispectra, Nonlinear Dyn. 25 (4) (2001) 383–393.
[32] P.T. Brewick, S.F. Masri, An evaluation of data-driven identification strategies for complex nonlinear dynamic systems, Nonlinear Dyn. 85 (2) (2016) 1297–1318.
[33] P.R. Crossley, J.A. Cook, A nonlinear engine model for drivetrain system development, Int. Conf. Control 2 (2002) 921–925.
[34] A. Vahidi, M. Druzhinina, A. Stefanopoulou, H. Peng, Simultaneous mass and time-varying grade estimation for heavy-duty vehicles, Proc. Am. Control Conf. 6 (2003) 4591–4956.
[35] M. Druzhinina, A.G. Stefanopoulo, L. Moklegaard, Speed gradient approach to longitudinal control of heavy-duty vehicles equipped with variable compression brake, IEEE Trans. Control Syst. Technol. 10 (2) (2002) 209–220.
[36] L. Moklegaard, M. Druzhinina, A. Stefanopoulou, Brake valve timing and fuel injection: a unified engine torque actuator for heavy-duty vehicles, Veh. Syst. Dyn. 36 (36) (2010) 179–201.
[37] J.B. Heyhood, Internal Combust. Engine Fundam. (1988).
[38] J. Chen, R.B. Randall, Improved automated diagnosis of misfire in internal combustion engines based on simulation models, Mech. Syst. Sig. Process. 64 (2015) 58–83.